Journal of the Korean Physical Society, Vol. 49, No. 4, October 2006, pp. 1667∼1674

Development of a Separation Algorithm for Peak Signals and Its Application to Event-Related Brain Potentials

Byung-Il Yoo* and Sooyong Kim
Department of Physics, Korea Advanced Institute of Science and Technology, Daejeon 305-701

Seungjin Choi
Department of Computer Science, Pohang University of Science and Technology, Pohang 790-784

Young Youn Kim
Institute for Neuroscience, Seoul National University College of Medicine, Seoul 110-744

Jun Soo Kwon
Department of Psychiatry, Seoul National University College of Medicine, Seoul 110-744 and Institute for Neuroscience, Seoul National University College of Medicine, Seoul 110-744

(Received 7 June 2006, in final form 19 July 2006)

The electrical activities of neuronal populations in the brain manifest as complex signals that can be recorded as a time series of electric potential differences on the human scalp. An event-related brain potential (ERP) is a peculiar feature in the signals, which is evoked by a specific stimulus or task, the so-called 'event'. The ERP contains a considerable number of distinct meaningful peak components that reflect brain functions related to the event. The complexity of the ERP can be easily characterized if it can be reliably decomposed into its subcomponents, thereby enabling the localization of the equivalent dipole sources corresponding to those components. To date, this decomposition has typically been performed using independent component analysis (ICA) or principal component analysis (PCA), both of which exploit the statistical independence or uncorrelatedness of sources. However, the temporally overlapped, distinct single-peak-pulse (SPP) signals within a time series are not only mutually dependent but also mutually correlated. In this paper, we propose a gradient descent method for the blind separation of dependent peak signal sources. The method does not exploit any statistical properties of the sources; rather, it uses simple functions characterizing the shapes of the output waveforms and an adaptive peak-searching technique. Application of the proposed method to a numerical example and data from a real ERP experiment suggest that it is superior to an ICA in terms of extracting peak component sources.

PACS numbers: 87.80.Tq
Keywords: Blind-source separation (BSS), Event-related Potentials (ERP), Single-pulse peak (SPP)

I. INTRODUCTION

The electrical signals generated by the living human brain are typical examples of a time series of high complexity. The brain contains an enormous number of neurons organized in complicated networks. Interactions between these neurons and their spontaneous activation concomitant with electrical activities give rise to membrane currents [1]. The electrical activities of relatively large neuronal populations manifest themselves as time-varying electric potential differences on the human scalp (-100 to 100 μV), which are recorded in the form of electroencephalograms (EEGs). EEGs, thus, contain a great deal of information on the neuronal activities in the brain. However, unscrambling this information is made difficult by the high complexity of EEG signals. For this reason, much research into the physics of brain potentials has been devoted to the nonlinear structural or the spectral analysis of EEG data [2–4]. However, although these approaches are useful for investigating the state of the brain at relatively large time scales, they cannot extract the rich information contained in EEGs.

An interesting feature in EEGs is the so-called event-related potential (ERP), which is the electrical activity of the brain time-locked to a specific stimulus or task, referred to as an 'event'. An analysis of ERPs provides detailed information with high temporal resolution that

*E-mail: biyoo@kaist.ac.kr; Fax: +82-42-869-2510

supplements the knowledge gained from functional magnetic resonance imaging (fMRI) and positron emission tomography (PET), which have poor time resolution. To obtain pure event-related signals, researchers usually average over a number of EEG trials time-locked to repetitive events, an approach that assumes that the background EEG can be considered as noise that will cancel out. However, ERPs are still complex because they are comprised of several oscillatory components caused by stimulus-induced changes in the EEGs [5–8] as well as numerous functionally meaningful distinct peak components generated from localized regions in the brain [9]. Furthermore, each ERP contains components arising from many regions at approximately the same time. From a physical viewpoint, if a method can be found to reliably decompose ERPs into their components, the complexity of ERPs may be easily characterized. Once the separated components are obtained, it would be possible to reconstruct the equivalent dipole sources corresponding to those components by using the electric potential distribution of the components on the scalp. This is one of the most important aspects of ERP analysis. Thus far, this decomposition has typically been performed through a blind source separation (BSS) method [10], such as an independent component analysis (ICA) [11–14] or a principal component analysis (PCA) [15–17].

In general, ICA and PCA exploit either the statistical independence or the uncorrelatedness of sources [10,18]. However, time series comprised of temporally overlapped single-peak-pulse (SPP) signals, such as the statistically dependent, but functionally distinct, meaningful peak components in ERPs, are not only mutually dependent but also mutually correlated. Despite the fundamental shortcomings of BSS methods and their inevitable inaccuracy for ERP analysis, these methods are still widely used for separating ERPs, even their dependent SPP components [11,14].

In this paper, we present a gradient descent method for separating dependent SPP sources contained in a linear multivariate mixture of SPP and non-SPP sources. Similar to an ICA, the framework of the proposed method is a gradient descent neural network (see Ref. 10 or Section II). We propose a fitness function based on simple functions characterizing the shape of the output waveforms and develop a gradient learning method with functionally extended learning rates that vary according to the distances from the estimated peak positions. Through a numerical example, we demonstrate that the proposed method can separate strongly dependent SPP sources with excellent performance whereas the ICA fails to separate the same sources. To examine the applicability of the proposed method, we apply the proposed method to real ERP data from a word repetition experiment [19]. We show that the locations of the equivalent dipoles corresponding to the separated components determined by the proposed method agree with the results of previous brain imaging studies related to word repetition effects. In those studies, fMRI [20] and low-resolution electromagnetic tomography (LORETA) here applied [19].

II. THE SEPARATION MODEL

The simplest form of BSS considers the following linear data model:

$$x_{kj} = \sum_{r=1}^{M} a_{kr} s_{rj},\ (k = 1, 2, \cdots, M; j = 1, 2, \cdots, N), \quad (1)$$

where M is the number of channels, N is the sample size (the index j, thus, corresponds to the discrete time t of the time series), the x_{kj}, s_{rj} and a_{kr} are the (k, j)-, (r, j)- and (k, r)-components of the $M \times N$ observed data matrix $\mathbf{X}$, the $M \times N$ unknown source matrix $\mathbf{S}$, and $M \times M$ unknown linear mixing matrix $\mathbf{A}$, respectively. The problem of BSS involves finding a demixing weight matrix $\mathbf{W}$ (whose components are denoted by w_{ik}) in a linear neural network such that the components of output $\mathbf{U}$,

$$u_{ij} = \sum_{k=1}^{M} w_{ik} x_{kj},\ (i = 1, 2, \cdots, M; j = 1, 2, \cdots, N), \quad (2)$$

correspond to a scaled and permuted source signal s_{rj}.

In the gradient-descent learning method for BSS, the separation is achieved by minimizing a *fitness function* (Ψ) that is to be defined such that the $\mathbf{W}$ is adjusted to a demixing matrix when the function Ψ is minimized; *i.e.*, the learning rule is formulated as

$$\begin{cases} w_{ik} \leftarrow w_{ik} + \Delta w_{ik} \\ \Delta w_{ik} = -\epsilon \frac{\partial \Psi}{\partial w_{ik}} \end{cases}, \quad (3)$$

where ϵ is the learning rate, which is set to a small value ($<$0.005) and prevents sudden changes in W. In infomax ICA [21] for example, which is known to have the simplest approach to deriving a general ICA learning rule, the negative of the entropy of the output signals is used as a fitness function (*i.e.*, maximizing the output information). In general, using a sigmoidal nonlinear function $g(\cdot)$(*e.g.*, $\tanh(\cdot)$), one can use a nonlinear transformed output

$$y_{ij} = g(u_{ij}) \quad (4)$$

to efficiently minimize the fitness function Ψ.

In the present model, we assume that the sources include distinctive SPP components, where the number of SPP sources does not exceed the number of sensor signals, M. The goal is to blindly separate these SPP sources. An ICA is the most useful tool for separating multi-channel source signals from their mixtures. However the goal of an ICA is to find statistically mutually independent outputs U given only mixed data X. In the case of separating dependent sources, ICA may give mutually independent outputs that do not correspond to the original sources. A special example of such sources

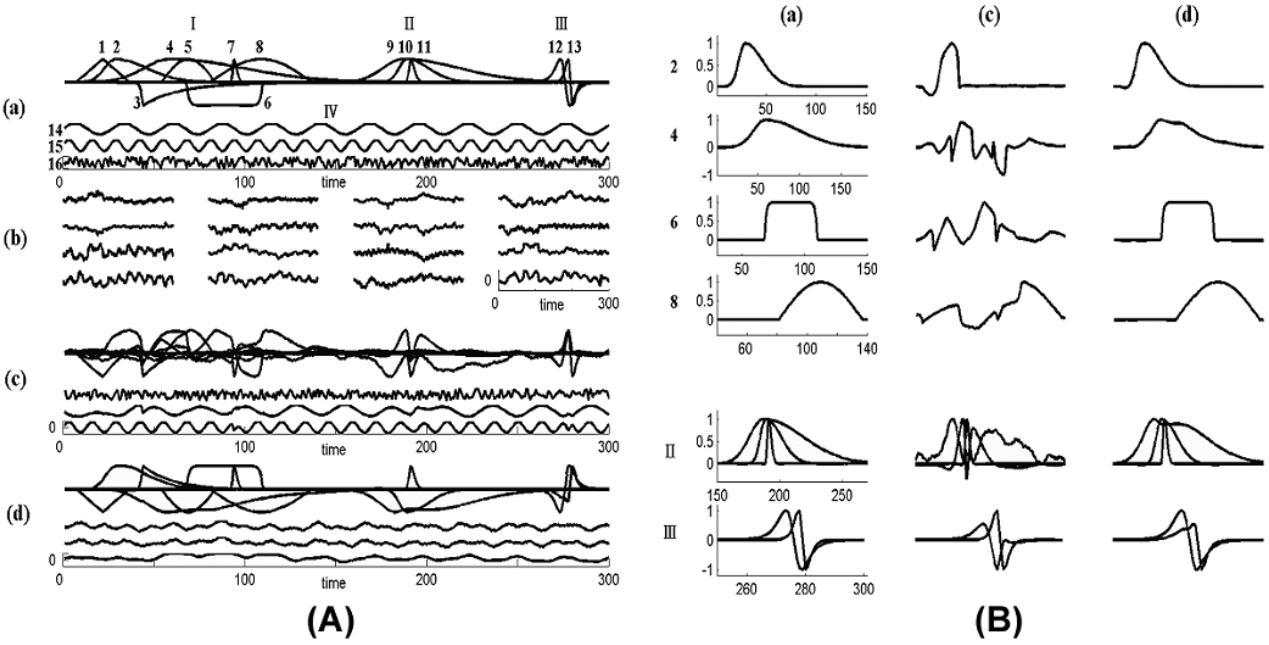

Fig. 1. (A) Illustration of the separation of 16-channel signals: (a) sources (11 SPPs, 2 sine waves, 1 white noise), (b) mixture in a 16 × 16 random matrix, (c) results of the ICA, (d) results of the proposed method. (B) Nine selected components from (A) (Note that mixtures (b) are omitted in (B)).

is temporally overlapped SPP sources. For a clear and intuitive understanding of the problem, we present a numerical example.

Fig. 1 illustrates a comparison of the results obtained by applying an ICA and the method proposed in this paper to a signal comprised of 16 mutually dependent component sources. Fig. 1(A)(a) shows the 16 mutually dependent component sources. The Arabic and Roman numerals indicate the channels (components) and groups, respectively. The sources consist of four test groups: overlapped multiform SPPs (I), wholly overlapped SPPs having nearly identical peak positions (II), overlapped double-peak impulses (III), and repetitive oscillatory waves and white noise (IV). The multiform SPPs are constituted by exponentially decaying (3), half sine (5,8), trigonal (1), square-like (6), and impulse-type peak (2,4,7) waves. The mixtures were constructed using a randomly generated 16 × 16 mixing matrix (Fig. 1(A)(b)). Better results were selected individually from the results of the infomax-ICA [21] (1-13) and extended-infomax-ICA [23] (14-16) methods (Fig. 1(c)). For a more detailed comparison, nine selected components from the same results are plotted in Fig. 1(B) (mixtures (b) are omitted in this figure). In the case of repetitive oscillatory waves and white noise (Group IV), the ICA provided relatively good results. In the case of the SPP components (1-11), however, ICA cannot separate the mixture of overlapped SPP sources due to their statistical dependence. This example highlights the need for a new method for separating statistically dependent SPP sources.

III. PROPOSED METHOD

To achieve BSS of statistically dependent SPP sources, we consider a fitness function Ψ_i for the i-th SPP component and a new type of gradient learning rule as follows:

$$\Psi_i = \sum_{l=1}^{L} \sum_{j=1}^{N} \psi_{ij}^{[l]} (l = 1, 2, \cdots, L) \tag{5}$$

$$\begin{cases} w_{ik} \leftarrow w_{ik} + \Delta w_{ik} \\ \Delta w_{ik} = -\sum_{l=1}^{L} \sum_{j=1}^{N-1} \epsilon_{ij}^{[l]} \frac{\partial \psi_{ij}^{[l]}}{\partial w_{ik}} \end{cases} \tag{6}$$

where $\psi_{ij}^{[l]}$ are the functions of the i-th output and are assumed to characterize the shapes of the output waveforms (*e.g.*, $\psi_{ij}^{[l]} = \psi_{ij}^{[l]}(\mathbf{Y})$), and $\epsilon_{ij}^{[l]}$ are the variable learning rates for $\psi_{ij}^{[l]}$ - named the *weighted learning rates* and formed into an $M \times N$ matrix - and are determined by using the estimated peak positions and peak widths of the SPP outputs (*i.e.*, the start, the end, and the peak positions of the SPP outputs; see Fig. 2(A) for an example). Once the candidates of $\psi_{ij}^{[l]}$ and $\epsilon_{ij}^{[l]}$ have been chosen, if even by a vague conjecture regarding their forms, one may check the optimal shape of the waveform for the learning rule that tries to separate the components of the waveform by using the criterion of minimizing Ψ_i. This check is achieved by solving the Euler equation [22] numerically with the boundary conditions imposed on the start, the end, and the peak points:

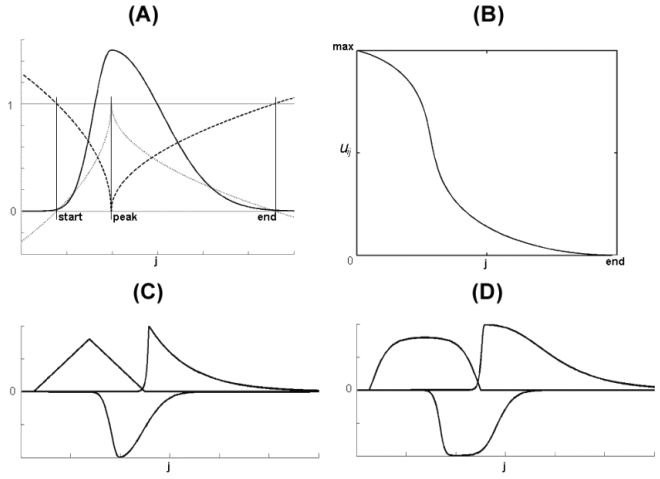

Fig. 2. (A) Illustration of the weighted learning rates for one of the M channels. (Solid, dashed and dotted lines indicate an example of an estimated SPP, and the corresponding $\epsilon_{ij}^{[2]}$ and $\epsilon_{ij}^{[3]}$, respectively). (B) One of the solutions of the Euler equation for the fitness function. (C) Three original SPP waveforms. (D) Illustration of the nonlinear transform of (C) by using Eq. (9) or (10) for $h^{[l]} = 3$.

$$\sum_{l=1}^{L} \epsilon_{ij}^{[l]} \frac{\partial \psi_{ij}^{[l]}}{\partial u_{ij}} - \frac{d}{dt} \sum_{l=1}^{L} \epsilon_{ij}^{[l]} \frac{\partial \psi_{ij}^{[l]}}{\partial u'_{ij}} = 0, \tag{7}$$

where u'_{ij} is du_{ij}/dt (in the discrete formula d/dt is dealt with as the difference with respect to increasing j). The solution u_{ij}, then, corresponds to the waveform of optimal shape for the learning rule. If a nonlinear transform $y_{ij}^{[l]} = y_{ij}^{[l]}(u_{ij})$, which makes the shapes of arbitrary SPP waveforms closer to optimal shapes for the separating criterion, can be defined, a learning rule for SPP can be successfully constructed.

Now, we present a simple, but generally usable, set of $\psi_{ij}^{[l]}$, $y_{ij}^{[l]}$, and $\epsilon_{ij}^{[l]}$ for separating SPP sources. The $\psi_{ij}^{[l]}$ and $y_{ij}^{[l]}$ are

$$\psi_{ij}^{[1]} = \sqrt{(y_{i(j+1)}^{[1]} - y_{ij}^{[1]})^2 + (\Delta\tau)^2},\ y_{ij}^{[1]} = u_{ij}, \tag{8}$$

$$\psi_{ij}^{[2]} = 2|y_{ij}^{[2]}|\Delta\tau,\ y_{ij}^{[2]} = |u|_i^{max} \tanh(h^{[2]} u_{ij}/|u|_i^{max}) / \tanh(h^{[2]}), \tag{9}$$

$$\psi_{ij}^{[3]} = -(y_{ij}^{[3]})^2\Delta\tau,\ y_{ij}^{[3]} = |u|_i^{max} \tanh(h^{[3]} u_{ij}/|u|_i^{max}) / \tanh(h^{[3]}), \tag{10}$$

where $\Delta\tau$ is the scaled sampling-time interval (to be dealt with later in the Section), $|u|_i^{max}$ is the maximum absolute value of the i-th output channel, and $h^{[l]}$ are the slope control parameters of the sigmoidal function $y_{ij}^{[l]}$. The $\epsilon_{ij}^{[l]}$ are

$$\epsilon_{ij}^{[1]} = \epsilon_0^{[1]} \quad (for\ all\ j), \tag{11}$$

$$\epsilon_{ij}^{[2]} = \begin{cases} \epsilon_0^{[2]} \sqrt{d_{ij}/d_i^L} & (for\ j \le j_i^{peak}) \\ \epsilon_0^{[2]} \sqrt{d_{ij}/d_i^R} & (for\ j > j_i^{peak}) \end{cases}, \tag{12}$$

$$\epsilon_{ij}^{[3]} = \begin{cases} \epsilon_0^{[3]} - \epsilon_0^{[3]} \sqrt{d_{ij}/d_i^L} & (for\ j \le j_i^{peak}) \\ \epsilon_0^{[3]} - \epsilon_0^{[3]} \sqrt{d_{ij}/d_i^R} & (for\ j > j_i^{peak}) \end{cases}, \tag{13}$$

where $\epsilon_0^{[l]}$ are the conventional learning rates, j_i^{peak} is the value of j at $|u|_i^{max}$, d_{ij} is the distance from j_i^{peak} in the space of index j (*i.e.*, $|j_i^{peak} - j|$), and d_i^L and d_i^R are the d_{ij} values at the start and the end points of the i-th current output peak, respectively. To evaluate d_{ij} and d_i^L, we search for a pair of j values for which the values of $y_{ij}^{[l]}$ are equal to 10 % of $|u|_i^{max}$ on the left and the right sides of the i-th peak; these j values are denoted $j_i^{L10\ \%}$ and $j_i^{R10\ \%}$, respectively. d_i^L and d_i^R are estimated by linear approximations, that is, $|j_i^{peak} - j_i^{L10\ \%}|/0.9$ and $|j_i^{peak} - j_i^{R10\ \%}|/0.9$, respectively. However, empirical results revealed that expanding the interval by 20 % gave superior results for SPPs with long tails. Hence, the expanded d_i^L and d_i^R are set to $|j_i^{peak} - j_i^{L10\ \%}|/0.75$ and $|j_i^{peak} - j_i^{R10\ \%}|/0.75$, respectively.

Fig. 2(A) illustrates an example of $\epsilon_0^{[2]}$ and $\epsilon_0^{[3]}$. Fig. 2(B) shows a numerical solution of Eq. (7), $\mathbf{u}_i(t)$, on the right side of the peak interval with boundary conditions at the peak and the end points. This argument does not imply that a specific fitness function can be used only for a specific optimal waveform, as diverse types of SPP sources are well separated using this criterion. However, the performance of the separation is improved by using outputs transformed by Eq. (9) or (10). The transform for $h^{[l]} = 3$ makes the shapes of the arbitrary SPP waveforms closer to the waveform illustrated in Fig. 2(B). Fig. 2(C) and (D) show examples of the transform of three representative SPP waveforms by Eq. (9) or (10) for $h^{[l]} = 3$. To derive the final learning rules, one computes the derivative of $\psi_{ij}^{[l]}$ with respect to w_{ik} as follows:

$$\partial\psi_{ij}^{[1]}/\partial w_{ik} = (u_{i(j+1)} - u_{ij})(x_{k(j+1)} - x_{kj})/\psi_{ij}^{[1]}, \tag{14}$$

$$\partial\psi_{ij}^{[2]}/\partial w_{ik} = 2[h^{[2]} \mathrm{sech}^2(h^{[2]} u_{ij}/|u|_i^{max}) / \tanh(h^{[2]})]\mathrm{sign}(u_{ij}) x_{kj}\Delta\tau, \tag{15}$$

$$\partial\psi_{ij}^{[3]}/\partial w_{ik} = -2[h^{[3]} \mathrm{sech}^2(h^{[3]} u_{ij}/|u|_i^{max}) / \tanh(h^{[3]})] y_{ij}^{[3]} x_{kj}\Delta\tau, \tag{16}$$

where $\mathrm{sign}(u_{ij})$ equals -1 for negative u_{ij} and 1 for non-negative u_{ij}.

As the learning rule has no convergence property, $\mathbf{W}$ is normalized such that $|det\mathbf{W}|$ equals 1 in each learning step. The '*natural gradient*' is applied to minimize the fitness function more efficiently [23]. This gradient rescales the Euclidian gradient so as to increase the

Table 1. Comparison of the error angles (in radians).

Component	1	2	3	4	5	6	7	8	9	10	11
ICA Algorithm	0.14	0.17	0.15	0.77	0.08	0.48	0.01	0.22	0.65	0.32	0.01
Proposed Algorithm	0.00	0.05	0.06	0.48	0.00	0.00	0.00	0.02	0.15	0.01	0.00

convergence efficiency. The natural gradient within the nonorthonormal space of $\mathbf{W}$ is known to be equivalent to the Euclidian gradient postmultiplied by $\mathbf{W}^T\mathbf{W}$ due to the Riemannian structure of the space of nonsingular square matrices [23]. The slope-control factors ($h^{[l]}$) in Eq. (9) and (10) are set to 3. The ratio of conventional learning rates $\epsilon_0^{[1]}$:$\epsilon_0^{[2]}$:$\epsilon_0^{[3]}$ in Eq. (11) $\sim$ (13) was set to 1:1:1 in this study. Their optimal values might depend on the shapes of the SPP sources and on their relative positions in some cases. However, it is remarkable that the proposed algorithm exhibits considerable flexibility (see Fig. 1; note that the separated components are not separated individually using the optimal parameters for each SPP waveforms). $\psi_{ij}^{[1]}$ in Eq. (8) can be expressed as $\sqrt{1+(y_{ij}^{[1]}/\Delta\tau)^2}\Delta\tau$. This quantity is not proportional to the scaled sampling time interval $\Delta\tau$ whereas $\psi_{ij}^{[2]}$ and $\psi_{ij}^{[3]}$ in Eq. (9) and (10) are proportional to $\Delta\tau$. Hence, the results obtained using the algorithm depend on $\Delta\tau$, although only weakly. A smaller value of $\Delta\tau$ is advantageous for data with wide peaks. If the width of the widest peak (number of samples from start to end of the peak) in the data to be separated is T, a value of $\Delta\tau$ that is greater than $1/T$ is favorable. $\Delta\tau$ was set to 0.003 in the present study.

To avoid unexpected edge effects due to incomplete waveforms at the two sample edges, we added a small number of zero values to the input vectors, $\mathbf{x}(t)$. The other processes followed the conventions that are commonly used for iterative gradient-descent algorithms [10, 24]. As we mentioned above, this method assumes that the number of SPP sources is no greater than the number of input channels, M; the input data sample needs to be segmented if this criterion is not met.

The performance of the proposed method can be checked by considering the numerical example presented in the previous section (Fig. 1). Fig. 1(d) shows the separation result obtained when the proposed method was applied to the mixed signal in Fig. 1(b). The results for the multiform SPPs (Group I) clearly show that the proposed method is sufficiently flexible to be applied to SPP waveforms with various shapes. The results obtained for the wholly overlapped SPPs having nearly identical peak positions (Group II) show better performance, which would not be expected for a method based on statistical properties. There was, however, some overreduction of the peaks of components 4 and 9 in Groups I and II, respectively. The results for the overlapped double-peak impulses (Group III) confirmed that the separation of the peaks had focused on only one of the two peaks, according to the criterion of single-peak separation. In the case of repetitive oscillatory waves and white noise (Group IV), the new method provided poorer results compared to the ICA. For a quantitative comparison of the separation performance, we calculated the error angles between the row vectors corresponding to each SPP component, where these vectors comprised the row components of the inverse of the mixing matrix (*i.e.*, $\mathbf{A}^{-1}$) and the sign-corrected row components of the resulting weights matrix (*i.e.*, $\mathbf{W}$ or $-\mathbf{W}$). The error angle becomes zero when the directions of the two row vectors are identical, and $\pi/2$ when they are orthogonal. Table 1 lists the error angles for the 11 SPP sources. The error angles for the proposed method are consistently smaller than those for the ICA, indicating that the proposed algorithm was more effective than the ICA in separating the dependent SPP sources.

IV. EXPERIMENTS AND RESULTS

To examine the applicability of the proposed method, we applied it to real ERPs related to the word repetition effect. To simplify this testing, an ERP data set from four right-handed healthy female subjects, aged 20 $\sim$ 26 years, was randomly selected from an ERP data set for 13 subjects that had been measured in a previous study [19]. Frequently used Korean noun words and pronounceable non-words were visually presented on a computer monitor to the subjects. The subjects were required to perform a word/non-word discrimination task by pressing a key with either their right or left index finger. The stimuli sets consisted of 120 words and 140 non-words that were presented only once, as well as 200 words that were repeated once. For the identical repeated words, the stimuli presented the first time are designated 'new words', and the later stimuli are designated 'old words'. These words were repeated after 1 $\sim$ 5 intervening words (new and old words). During the discrimination task, an EEG was recorded using a 128-channel Quik-cap system (Neuroscan, El Paso, TX, USA) with of analogue band-pass 0.05 $\sim$ 100 Hz and a sampling rate of 1000 Hz. To streamline the testing of the proposed method, we selected 19 channels (FP1, FP2, F7, F3, Fz, F4, F8, T7,

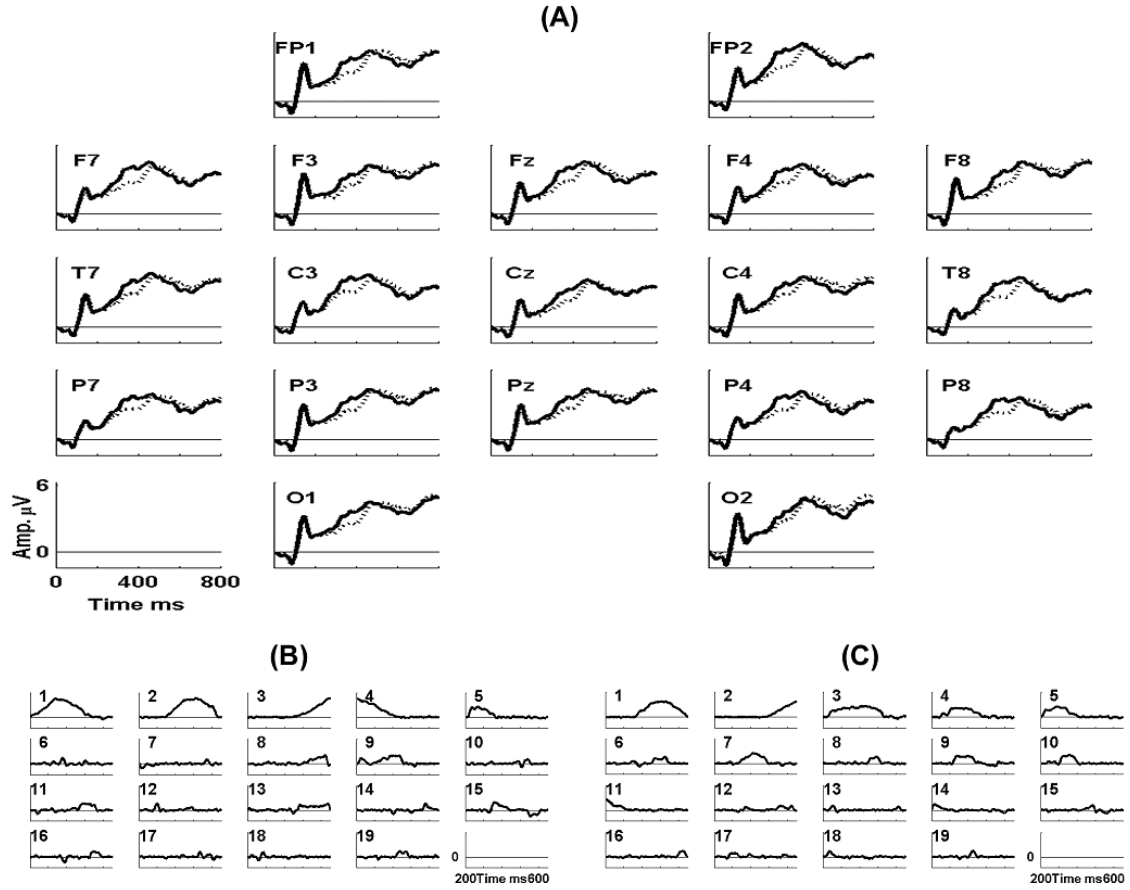

Fig. 3. Averaged ERPs and an illustration of the separation result. (A) Averaged ERPs elicited by old and new words at 19 electrode sites in the lexical decision task for all subjects (Dotted lines represent the ERPs for new words, and bold lines represent the ERPs for old words). (B) Separation results of the ERP for old words from 200 to 650 ms for Subject 1. (C) Results for new words.

C3, Cz, C4, T8, P7, P3, Pz, P4, P8, O1, O2) from the 128 EEG channels. The EEG recording for each subject was segmented into 1100-ms epochs only for the EEG of the correct responses on the discrimination task. The ERPs were obtained by averaging the EEG epochs for each subject and each stimulus presentation (old words and new words). The resulting ERPs were digitally filtered with a bandpass of 0.1 $\sim$ 30 Hz (see Ref. [19] for further details of the experiment).

Fig. 3(A) shows the averaged ERPs elicited by old and new words at 19 electrode sites for all subjects. Each graph in Fig. 3(A) is arranged according to the real electrode's site on the scalp. The old words elicited more positive ERPs compared to the new words. This word repetition effect began at about 200 ms post-stimulus and lasted until about 500 ms. However, the positive peak was located near 500 ms; hence, the end of the time interval was set to 650 ms instead of 500 ms. To separate the components causing the difference in the ERPs elicited by old and new words, we segmented the 19-channel ERPs over a time interval of 200 $\sim$ 650 ms and decomposed them by using the proposed method. Fig. 3(B) and (C) illustrate representative separation results of the ERPs elicited by the old and the new words, respectively, for one of the subjects.

Equivalent current dipoles were then sought for each of the resulting components by means of a dipole source localization routine [DIPFIT, contributed by Robert Oostenveld (F. C. Donders Centre, the Netherlands)] - as implemented in the open source toolbox EEGLAB with default parameter settings [25], by using a standard four-shell spherical head model (radii in mm: 71, 72, 79, 85; conductivity in S/m: 0.33, 1, 0.0042, 0.33). For each subject, 2 $\sim$ 11 fitted dipoles were found for the ERPs elicited by old words, and 4 $\sim$ 7 dipoles were found for those elicited by new words. Fig. 4(A) and (B) show the resulting equivalent dipoles of the corresponding components in Figs. 3(B) and (C), respectively. Previous fMRI [20] and LORETA [19] studies on word repetition effects found that the brain activations elicited by old words showing the greatest reduction were located in the left frontal area (Talairach coordinates [26], $-50 < x < -35$, $0 < y < 35$, $-10 < z < 25$, included in the Brodmann area (BA) 44/45/47 [20]). To determine whether the

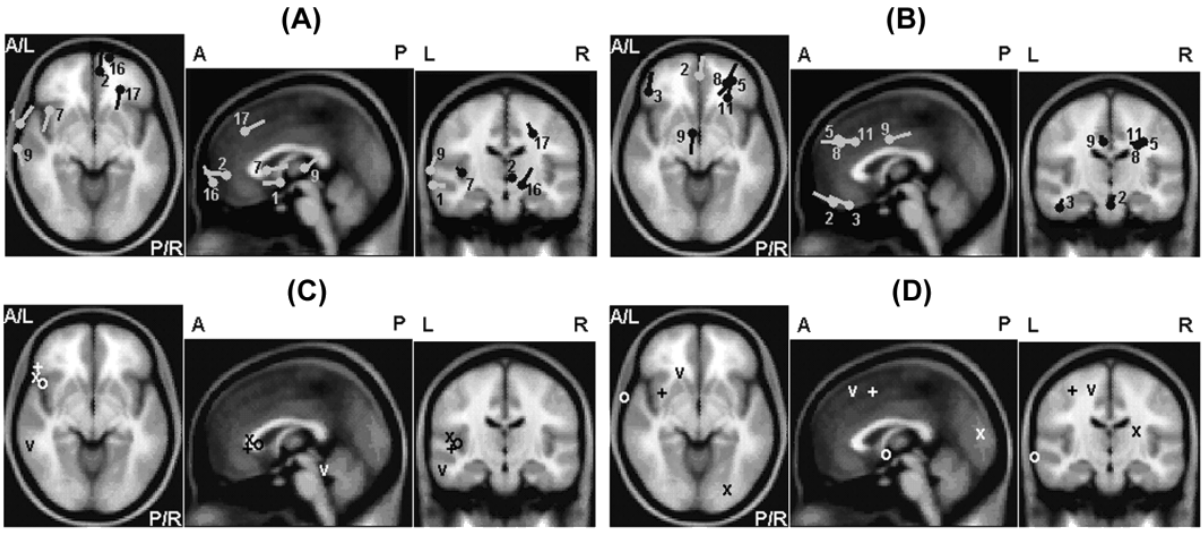

Fig. 4. Positions of equivalent dipoles of ERP components in the time range 200 ∼ 650 ms. (A) and (B) show the equivalent dipoles of old (A) and new (B) word ERP components obtained using the proposed method for Subject 1. The dipole numbers in (A) and (B) correspond to the component numbers in Fig. 3(B) and (C), respectively. In the results for new words (A), no dipoles exist in BA 44/45. Dipole 3 is located near BA 47; however, the z value of the Talairach coordinates of the dipole is out of the range of $-10 < z < 25$. In the results for old words (B), dipole 7 is located in BA 44/45/47. (C) and (D) show the positions of the fitted dipoles nearest to BA 44/45/47 for new word ERP components obtained using the proposed method (C) and ICA (D) for all subjects. (**o**: subject 1 - dipole 7 in (A), **x**: subject 2, +: subject 3, **v**: subject 4; A: anterior, P: posterior, L: left, R: right; BA: Brodmann Area; these images were generated using an EEGLAB open source toolbox, and the symbols indicating dipoles were modified).

results obtained using the proposed method agree with previous findings on word repetition effects, we sought for each subject dipoles located in these areas that exist only in the new word results.

For one of the four subjects, the dipoles were found neither in the results for the new words nor in those for the old words. For three of the four subjects, however, focused dipoles of this type were found (Fig. 4(C)). Furthermore, the separated ERP components corresponding to the dipoles of this type consistently commenced at a time in the range of 320 ∼ 350 ms. The agreement of the results obtained using the proposed method with previous findings confirms the applicability of the proposed method to a real ERP analysis. We also sought dipoles by using the separation results of infomax-ICA ('runica' routine in EEGLAB); however, these dipoles could not be found in the new word results for any of the subjects (Fig. 4(D)).

V. CONCLUSION

A new method for the separation of SPP sources in a linear multivariate mixture of such sources and non-SPP sources, developed for use in the decomposition of ERPs, is proposed. Although this method is based on a simple algorithm, its excellent performance was confirmed through a numerical example and by an experiment using real ERP data. The presented results suggest that the proposed method is superior to an ICA in terms of extracting SPP sources. The method, furthermore, does not require a large sample size, unlike methods based on statistical properties. In practical applications, however, real ERPs are not comprised solely of SPP sources. For this reason, when applying the proposed method, it is advisable to take the ICA or the PCA results into account, together with those of the proposed method. If an ERP can be decomposed completely, the complexity of the ERP may be easily characterized by examining the extracted components. Now, only the problem of separating dependent non-SPP sources blocks achieving the complete decomposition of ERPs.

Similar to the case of an ICA, in the proposed method, the assumption regarding the number of distinct sources affects the separation performance. If the number of input channels (*e.g.*, the number of sensor signals) is greater than the number of sources, the weight matrix will be a singular matrix. If, however, the measures contain sensor noise and residual background EEG noise, the proposed method will generate pseudo-components that are not an original source but an SPP produced by a linear combination of non-SPP waves. If, conversely, the number of input channels is less than the number of sources, some components will be deformed. The number of distinct sources can be controlled by adjusting the segmentation interval.

There is still room to improve the proposed method. As outlined in Fig. 1, the proposed method can sep-

arate SPP sources with arbitrary shapes. However, as observed for components 4 and 9 in Fig. 1(d), overreduction can occur for some SPP shapes under certain overlap conditions. In the present work, the learning rate ratio in Eq. (11) $\sim$ (13), $\epsilon_0^{[1]}$:$\epsilon_0^{[2]}$:$\epsilon_0^{[3]}$, was set to 1 : 1 : 1. In many cases, the overreduction problem can be solved by increasing $\epsilon_0^{[3]}$ in Eq. (13). However, a method that identifies the proper value of $\epsilon_0^{[3]}$ without any prior knowledge has not yet been developed. A modified hyperbolic tangent was adopted as the nonlinear function of the neural network. As in an ICA, it is possible to exploit multiple nonlinear functions according to the sources. If circumstances require, we can consider a new set of $\psi_{ij}^{[l]}$, $y_{ij}^{[l]}$, and $\epsilon_{ij}^{[l]}$. According to the designing of the function set, it is possible to construct a new algorithm for separating other types of components.

ACKNOWLEDGMENTS

The authors are grateful to Andrzej Cichocki and Te-Won Lee for helpful discussions and comments. This research is partially supported by a Korean Science and Engineering Foundation (KOSEF) Grant.

REFERENCES

[1] F. L. Silva, Electroenceph. Clin. Neurophysiol. **79**, 81 (1991).
[2] R. G. Andrzejak, K. Lehnertz, F. Mormann, C. Rieke, P. David and C. E. Elger, Phys. Rev. E **64**, 061907 (2001).
[3] G. Widman, T. Schreiber, B. Rehberg, A. Hoeft and C. E. Elger, Phys. Rev. E **62**, 4898 (2000).
[4] T. Gautama, D. P. Mandic and M. M. Hulle, Phys. Rev. E **67**, 046204 (2003).
[5] B. H. Jansen, G. Agarwal, A. Hegde and N. N. Boutros, Clin. Neurophysiol. **114**, 79 (2003).
[6] W. Klimesch, B. Schack, M. Schabus, M. Doppelmayr, W. Gruber and P. Sauseng, Brain Res. Cogn. Brain Res. **19**, 302 (2004).
[7] V. Kolev and J. Yordanova, Biol. Cybern. **76**, 229 (1997).
[8] S. Makeig, M. Westerfield, T. P. Jung, S. Enghoff, J. Townsend, E. Courchesne and T. J. Sejnowski, Science **295**, 690 (2002).
[9] M. G. H. Coles and M. D. Rugg, in *Electrophysiology of Mind*, edited by M. D. Rugg and M. G. H. Coles (Oxford University Press, Oxford, 1995), p. 1.
[10] A. Hyvaerinen, J. Karhunen and E. Oja, *Independent Component Analysis* (John Wiley & Sons, Inc. New York, 2001).
[11] S. Debener, S. Makeig, A. Delorme and A. K. Engel, Cognitive Brain Res. **22**, 309 (2005).
[12] S. Makeig, T. P. Jung, A. J. Bell, D. Ghahremani and T. J. Sejnowski, Proc. Natl. Acad. Sci. **94**, 10979 (1997).
[13] K. R. Muller, R. Vigario, F. Meinecke and A. Ziehe, Int. J. Bifurc. Chaos. **14**, 773 (2004).
[14] F. Piccione, F. Giorgi, P. Tonin, K. Priftis, S. Giove, S. Silvoni, G. Palmas and F. Beverina, Clin. Neurophysiol. **117**, 531 (2006).
[15] A. Beauducel, S. Debener, B. Brocke and J. Kayser, J. Psychophysiol. **14**, 226 (2000).
[16] M. Sotillo, L. Carretie, J. A. Hinojosa, M. Tapia, F. Mercado, S. Lopez-Martin and J. Albert, Neurosci. Lett. **373**, 5 (2005).
[17] K. Spencer, J. Dien and E. Donchin, Psychophysiology **36**, 409 (1999).
[18] S. Choi, A. Cichocki, H. Park and S. Lee, Neural Information Processing-Letters and Review **6**, 1 (2005).
[19] Y. Y. Kim, B. Lee, Y. W. Shin, J. S. Kwon and M. S. Kim, NeuroImage **29**, 712 (2006).
[20] D. I. Donaldson, S. E. Petersen and R. L. Buckner, Neuron **31**, 1047 (2001).
[21] A. J. Bell and T. J. Sejnowski, Neural Comput. **7**, 1129 (1995).
[22] G. Arfken, 1985. *Mathematical methods for physicsists.* 3rd Ed. Academic press, Orlando, Florida.
[23] S. Amari, A. Cichocki and H. H. Yang, in *NIPS'95*, Vol. 8 (MIT Press, Cambridge, 1996), p. 757.
[24] T. W. Lee, M. Girolami and T. J. Sejnowski, Neural Comput. **11**, 606 (1999).
[25] A. Delrme and S. Makeig, J. Neurosci. Meth. **134**, 9 (2004).
[26] J. Talairach and P. Tournoux, *Co-Planar Stereotaxic Atlas of the Human Brain: 3-Dimensional Proportional System-an Approach to Cerebral Imaging* (New York: Thieme Medical Publishers, 1988).